Nonlinear Large Deflection Analysis of Stiffened Plates

Khosrow Ghavami and Mohammad Reza Khedmati

Additional information is available at the end of the chapter

1. Introduction

Stiffened plates are basic structural members in marine structures as shown in Figure 1, and include also aeronautic and space shuttles among other structures. Due to the simplicity in their fabrication and high strength-to-weight ratio, stiffened plates are also widely used for construction of land based structures such as box girder and plate girder bridges. The stiffened plate has a number of one-sided stiffeners in either one or both directions, the latter configuration being also called a grillage (Figure 2). Ultimate limit state design of Stiffened plates' structures requires accurate knowledge about their behaviour when subjected to extreme loading conditions.

One of the most important loads applied on stiffened plates is the longitudinal in plane axial compression arising for instance from longitudinal bending of the ship hull girder as presented in Figure 3. The need to improve our knowledge of the buckling modes of such plates was emphasised after the collapse of several offshore structures and some ships in Brazil as well as the failure of several box girder bridges in the seventies of the twentieth century, Merrison Committee [1], Crisfield [2], Murray [3], Frieze, et.al. [4]. Stiffened plates are efficient structures, as a large increment of the strength is created by a small addition of weight in the form of stiffeners. However the collapse mechanisms of stiffened plates under predominantly compressive load present a complex engineering problem due to the large number of possible combinations of plate and stiffener geometry, materials, boundary conditions and loading. The design of such structure has to meet several requirements such as minimization of the weight and maximization of the buckling load. Thus, the designer of this structure is confronted with the problem of satisfying two conflicting objectives; such problems are called multi-objective or vector optimisation problems. In general, the objective-functions do not attain their optimum in a common point of the feasible points, Brosowski & Ghavami [5, 6].

INTECH
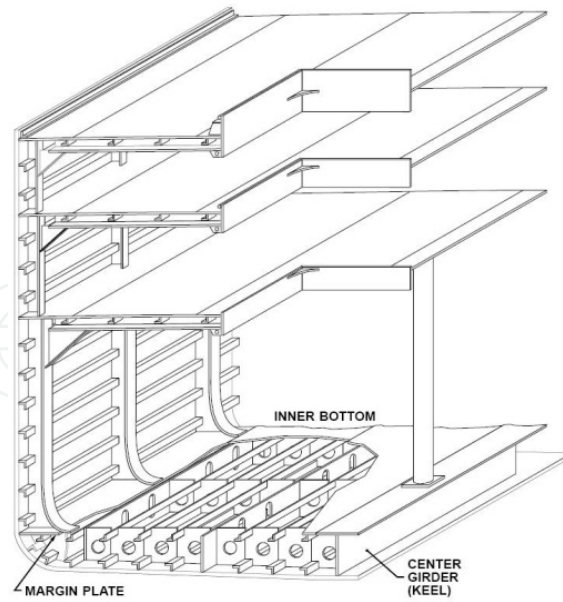open science | open minds

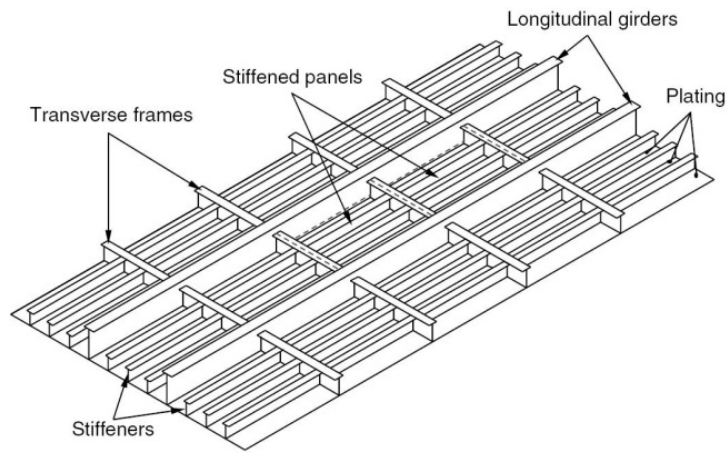**Figure 1.** Some examples of thin-walled structures

Figure 2. Structure of stiffened plates of the grillage type
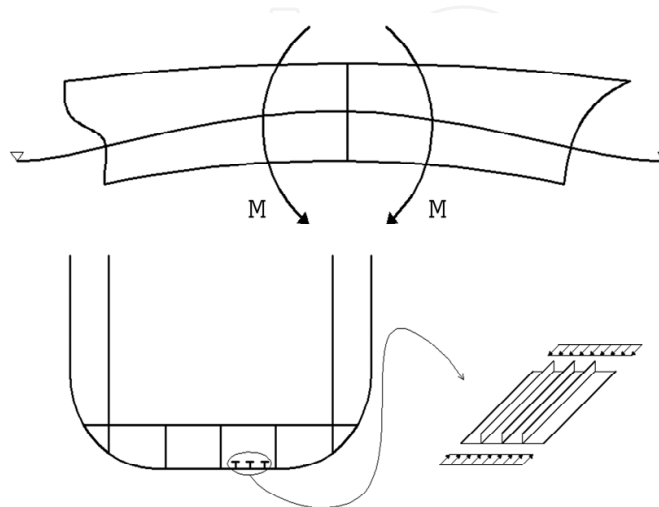

Figure 3. In-plane loading of stiffened plates when longitudinal bending of ship hull girder

For the analysis of such structural elements, the theory of orthotropic plate can be used to predict the global buckling stresses but not the local buckling and the interaction between the plate and the stiffeners, for the predominantly in-plane loading. In stiffened plates the initial imperfections due to the fabrication are inevitable. The buckling mechanism of stiffened plates depends, strongly, on the direction of initial bows, i.e. whether they are towards the plate or the stiffener. In the former case, the collapse is sudden due to buckling of the stiffener in contrast to the latter case, where a gradual failure occurs. Despite a substantial amount of theoretical research into the ultimate load behaviour of stiffened plates subjected to predominately in-plane loading, the accuracy and reliability of the predicted collapse load considering all the variables is not yet well confirmed. Specifically, in the available literature, no systematic theoretical and experimental investigation of the geometrical shape of the stiffeners cross-section on the ultimate buckling load behaviour of the stiffened plates, the interaction between the stiffeners and the plate, which was is the objectives of this chapter is being presented.

The buckling behaviour of stiffened plates under different loading conditions which has been the topic of the authors investigation, both experimentally and numerically, during last three decades has been reviewed concisely in this chapter. Chen et al. [7] carried out experimental investigations on 12 stiffened plates under in-plane longitudinal compression, purely or in combination with lateral load. The specimens were in different damage conditions: seven "as-built", two "dented" and three "corroded". Hu and Jiang [8] simulated some of the tests made by Chen et. al. [7], using the commercial program ADINA [9] and in-house program VAST [10], both based on the FEM. The former was used to analyse the "as-built" and "dented" stiffened plates, whereas the "corroded" specimens were analysed using VAST [4]. It was found, that in most cases the FEM produced similar responses to those of experimental results up to the loss of structural continuity. Grondin et al. [11] made a parametric study on the buckling behaviour of stiffened plates using the FEM-based commercial program ABAQUS [12]. Sheikh et. al. [13] extended the studies in [11] to investigate the combined effect of in-plane compression and bending using the same program. In these studies, only tee-shape stiffeners, plate aspect ratios, plate-to-stiffener cross-sectional area ratio with different initial imperfections of the plates were investigated.

All the cited studies, either experimentally or numerically, investigated the strength behaviour of longitudinally stiffened plates with specific boundary conditions. The continuity of both plates and stiffeners in thin-walled structures, composed of stiffened plates, leads to an interaction among the adjacent panels. Among the several available experimental investigations, two series of well executed experimental data on longitudinally multi-stiffened steel plates, with and without transversal stiffeners subjected to uniform axial in-plane load carried out to study the buckling and post-buckling up to final failure have been chosen. The first series are those of Ghavami [14] where the influences of stiffener cross-section of the type rectangular (R), L and T, as shown in Figure 4, have been investigated. The spacing of the stiffeners and the presence of rigid transversal stiffeners on the buckling behaviour up to collapse have also been studied. The second series of Tanaka &

Endo [15], where the behaviour of stiffened plates have three and two flat bars for longitudinal and transversal stiffeners respectively, were analysed. Besides, owing to the recent progress in the field of finite element method and available powerful FEM programs, it has been possible to assess the structural behaviour of the considered plates and stiffeners subjected to any combination of loads.
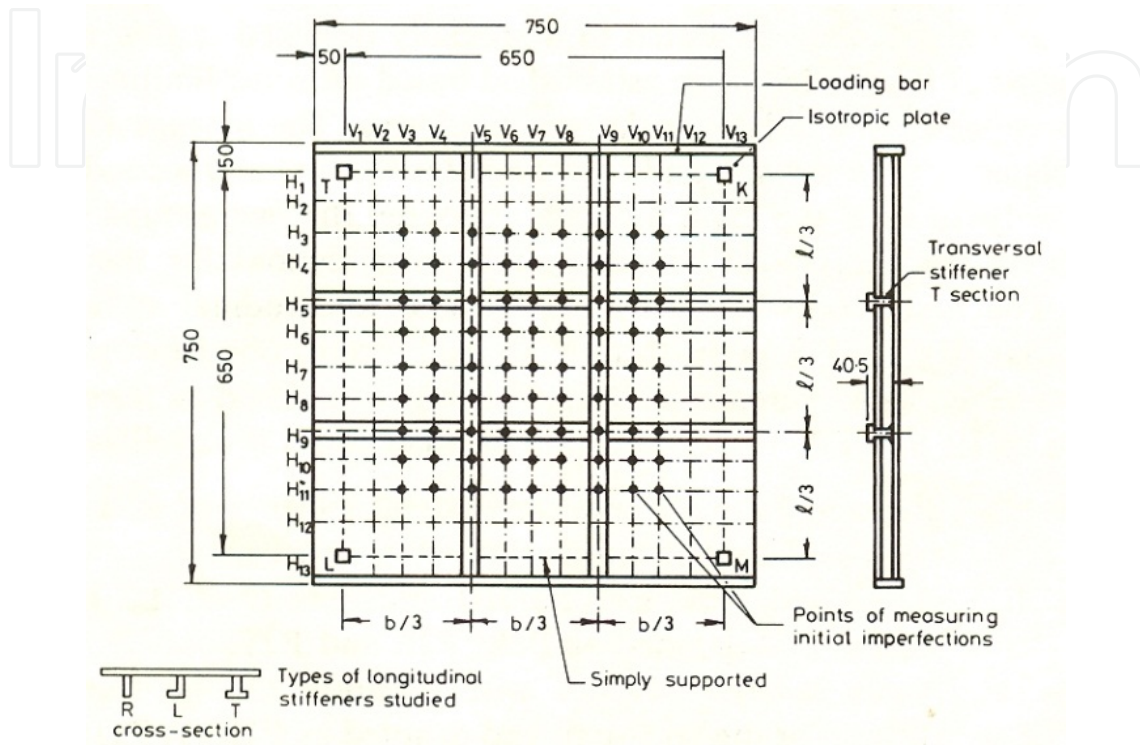

Figure 4. Ghavami's test models

Therefore one of the principal aims of this chapter is to present the applicability of the finite element method to simulate test results. The Finite Element Method (FEM) technique is employed to trace a full-range of elastic-plastic behaviour of the stiffened plates. It is seen that the FEM-based software is capable and accurate enough to simulate the test results. With the availability of high memory and high speed PCs', FEM programs become fast and cheap means to predict the buckling and post-buckling behaviour of stiffened plates with different configurations up to collapse. Successful simulations using FEM-based software means, that plate with different dimensions under various types of loading combinations and damages can be studied numerically. Besides, validated simulations using such programs enhance estimation of the ultimate strength analysis of box-like thin-walled structures composed of plates and stiffened plates.

2. Ghavami's experiments

Ghavami [14] tested a total number of 17 plate models of overall dimensions B=L=750 mm in a specially designed testing rig as shown in Figure 5. The models were divided into six series, with their definition and dimensions summarised in Tables 1 and 2. The average

thickness of the plate was t=4.4mm for the longitudinally stiffened plates with one and two rectangular (R), L and T stiffeners, designated as P1R, P1L, P1T and P2R, P2L, P2T respectively. The thickness of the plates, stiffened longitudinally, as for the series II and III but with one or two transversal stiffeners of T sections, P1R1T, P1L1T, P1T1T, P2R1T, P2L1T, P2T1T and P2R2T, P2L2T, P2T2T respectively was equal to 4.8mm. The span between the simple supports for all models was 650mm in both directions. In each group one isotropic plate, P1, P2 was also tested as a reference model. However the supports for the longitudinally stiffened plates, series II and III were not continuously simply supported but were very closely discretized simply supported and those with transversal stiffeners had continuously simply supported boundary conditions. A summary of material properties and test results is given in Table 3.
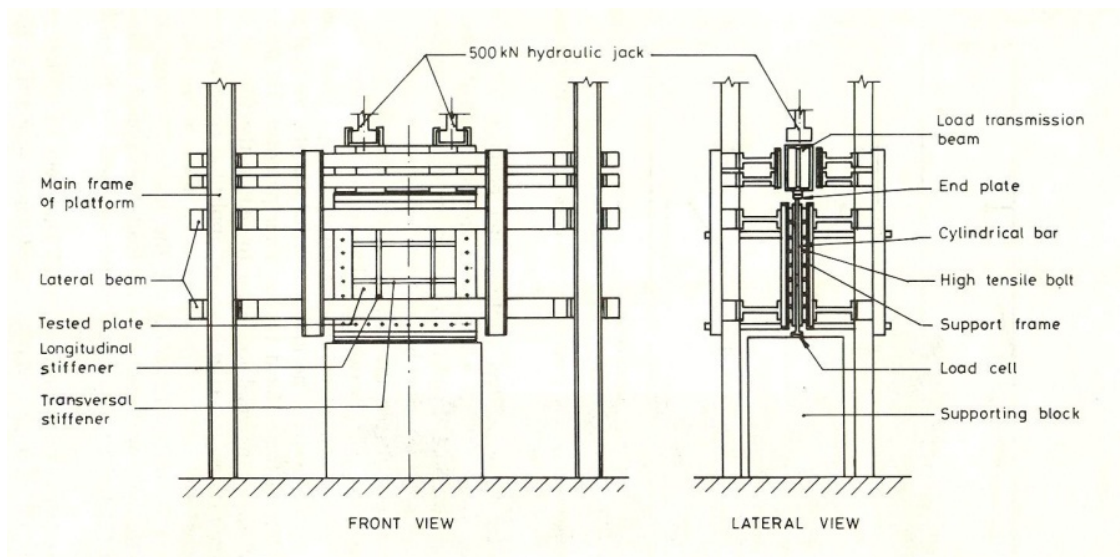

Figure 5. Ghavami's testing rig

Series No.	Definition	Test models
I	Unstiffened plate	P1, P2
II	Plate with one longitudinal stiffener of R, L and T cross-section	P1R, P1L, P1T
III	Plate with two longitudinal stiffeners of R, L and T cross-section	P2R, P2L, P2T
IV	Plate as series II but with addition of one transversal stiffener at the mid-span	P1R1T, P1L1T, P1T1T
V	Plate as series III but with addition of one transversal stiffener at the mid-span	P2R1T, P2L1T, P2T1T
VI	Plate as series II but with addition of two transversal stiffeners at 1/3 of span	P2R2T, P2L2T, P2T2T

Table 1. Definition of Ghavami test models

Test model	Plate			Longitudinal stiffener				Transverse stiffener			
	L	b	t	t_w	h_w	t_f	b_f	t_{wt}	h_{wt}	t_{ft}	b_{ft}
	mm	mm	mm	mm	mm	mm	mm	mm	mm	mm	mm
P1	650	650	4.4	----	----	----	----	----	----	----	----
P1R	650	325	4.4	7.0	30.0	----	----	----	----	----	----
P1L	650	325	4.4	6.4	30.0	3.9	16.4	----	----	----	----
P1T	650	325	4.4	6.4	30.0	4.8	26.4	----	----	----	----
P2R	650	217	4.4	7.0	30.0	----	----	----	----	----	----
P2L	650	216	4.4	6.4	30.0	19.5	16.4	----	----	----	----
P2T	650	217	4.4	6.4	30.0	20.0	26.4	----	----	----	----
P2	650	650	4.8	----	----	----	----	----	----	----	----
P1R1T	325	325	4.8	5.1	30.0	----	----	4.7	41.1	4.1	35.3
P1L1T	325	325	4.8	5.2	30.2	3.4	14.8	4.8	40.4	4.1	34.2
P1T1T	325	325	4.8	4.6	30.0	3.8	25.3	4.9	40.4	4.2	35.2
P2R1T	325	216	4.8	5.1	30.0	----	----	4.7	40.7	3.8	35.7
P2L1T	325	217	4.8	5.1	30.2	17.2	14.6	4.6	40.6	4.1	35.9
P2T1T	325	217	4.8	4.7	28.8	13.5	25.0	4.7	39.6	4.1	34.8
P2R2T	216	216	4.8	5.0	30.1	----	----	4.7	40.4	4.1	35.7
P2L2T	217	217	4.8	5.1	30.0	17.0	14.9	4.7	40.6	4.1	35.5
P2T2T	216	216	4.8	4.6	29.8	13.0	24.8	4.8	40.6	4.1	35.5

Table 2. Dimensions of plate and stiffeners in Ghavami test models

The testing rig was constructed within the Structural and Material Laboratory of PUC-Rio and is shown in Figs. 5 and 6. Out of plane deflections of plates and stiffeners were measured principally by mechanical dial gauges fixed at specific points mounted on the testing rig, as shown in Figure 6. In all models electrical linear strain gauges or rosettes measured the strains. More details on the test rig, test models and the process of the tests can be found in reference [14]. In each test the maximum ultimate collapse stress σ_{ult} was calculated by dividing the ultimate load P_u to the overall cross-section of the plate A_p and stiffeners A_s as given by eqn (1):

$$\sigma_{ult} = P_u / \left(A_p + A_s \right) \tag{1}$$

The squash load P_{sq} was calculated by multiplying the yield stress of the plate σ_{Yp} and the stiffener σ_{Ys} with their appropriate cross-section areas as eqn (2):

$$P_{sq} = \sigma_{Yp} A_p + \sigma_{Ys} A_s \tag{2}$$

The test results together with those of maximum initial W_0, final W_{max} deflections and in-plane shortening U_{max} are given in Table 3.

Test model	Material properties			Measured deflection	Maximum deflection	Maximum shortening	Collapse stress
	E	σ_{Yp}	σ_{Ys}	$W_o\,/\,t$	$W_{max}\,/\,t$	$U_{max}\,/\,t$	$\sigma_{ult}\,/\,\sigma_{Yp}$
	$MPa \times 10^5$	MPa	MPa	%	%	%	%
P1	1.81	218	----	61	278	0.38	42.2
P1R	1.81	218	390	69	188	0.31	70.2
P1L	1.99	227	270	36	123	0.34	66.5
P1T	1.99	227	170	9	33	0.27	60.0
P2R	1.95	224	390	25	117	0.41	66.0
P2L	2.21	223	270	19	142	0.30	74.0
P2T	2.21	223	270	3	128	0.37	74.0
P2	1.78	220	----	20	121	0.40	48.2
P1R1T	1.85	219	326	21	123	0.33	74.0
P1L1T	1.91	225	326	27	27	0.48	71.1
P1T1T	1.75	219	273	33	121	0.33	72.1
P2R1T	1.75	219	326	70	52	0.64	88.6
P2L1T	1.89	227	326	40	33	0.60	84.6
P2T1T	1.78	220	273	23	30	0.51	89.1
P2R2T	1.91	225	326	32	18	0.63	86.2
P2L2T	1.89	227	326	28	53	0.56	97.4
P2T2T	2.09	218	273	32	16	0.51	103.2

Table 3. Summary of material properties and results for Ghavami test models
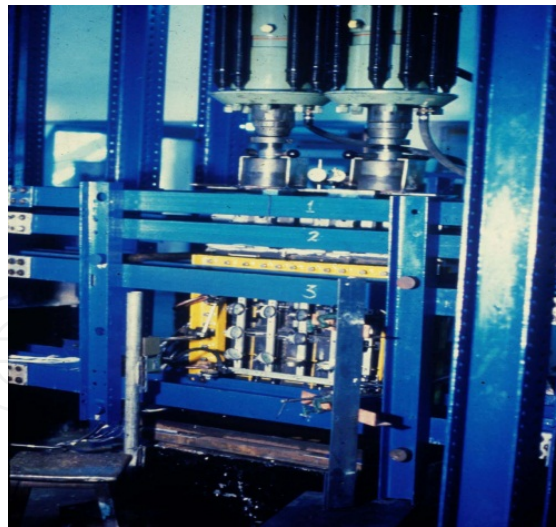

Figure 6. Stiffened plate model positioned in the Ghavami's testing rig

3. Tanaka & Endos' experiments

Tanaka & Endo [15] carried out a series of experimental and numerical investigations on the ultimate compressive strength of plates having three and two flat-bars stiffeners welded longitudinally and transversally respectively. A total of 12 tests were performed. The test

specimen was designed so that the longitudinally stiffened plates located in the middle of whole test specimens could fail. The test specimens were intended to fail by local plate buckling or tripping of longitudinal stiffeners. A typical test rig from the Tanaka & Endo study is shown in Figure 7. A stiffened plate model positioned in their testing rig is presented schematically in Figure 8. To account for the effect of adjacent panels on the collapse behaviour of central panel, three-span models with two adjacent (dummy) stiffened panels and supported by two transverse frames were employed. The thickness of plate and stiffeners in two adjacent panels was 1.2-1.3 times that of plate and stiffeners in the central panel. Table 4, where a=1080mm is the span length of the plate with average plate thickness between t=4.38mm to t=6.15mm, represents geometric and material properties for the Tanaka & En'os' test structures. The boundaries of stiffened plates were continuously simply supported and the in-plane axial compression load was applied longitudinally. The maximum measured initial deflections in the plate were ranging between 0.1-0.4 mm. The ultimate collapse strength and squash load were calculated in the same manner using equations 1 and 2 as those considered by Ghavami [14].

Structure No.	a (mm)	b (mm)	t (mm)	h_w (mm)	t_w (mm)	$\dfrac{h_w}{t_w}$	A_{03} (mm)	σ_{Yp} (MPa)	σ_{Ys} (MPa)	E (GPa)
D0		1440	6.15	110.0	9.77	11.26	0.101	234.2	287.1	205.8
D0A		1440	5.65	110.0	10.15	10.84	0.250	249.9	196.0	205.8
D1		1200	5.95	110.0	10.19	10.79	0.143	253.8	250.9	205.8
D2		1560	5.95	110.0	10.19	10.79	0.288	253.8	250.9	205.8
D3	1080	1440	5.95	103.5	11.84	8.74	0.312	253.8	326.3	205.8
D4		1440	5.95	118.5	7.98	14.85	0.119	253.8	284.2	205.8
D4A		1440	5.65	118.5	8.08	14.67	0.379	249.9	274.4	205.8
D10		1200	4.38	65.0	4.38	14.84	0.515	442.0	442.0	205.8
D11		1200	4.38	90.0	4.38	20.55	0.503	442.0	442.0	205.8
D12		1440	4.38	65.0	4.38	14.84	0.523	442.0	442.0	205.8

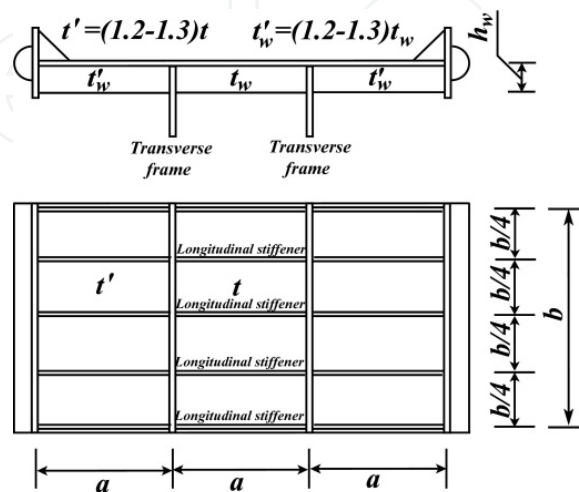**Table 4.** Geometric and material properties of Tanaka & Endo tests
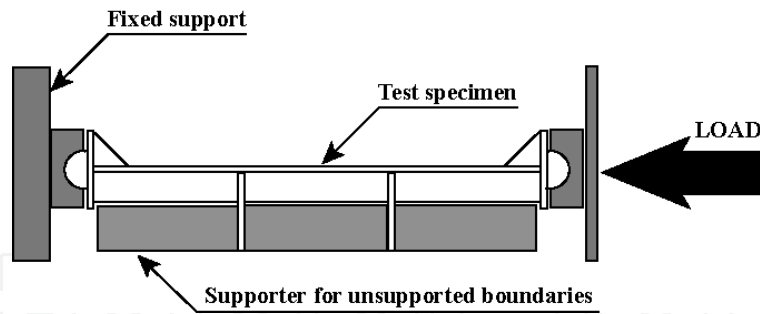

Figure 7. Tanaka & Endo's test model

Figure 8. Stiffened plate model positioned in the Tanaka & Endo's testing rig

4. Finite element simulations

Since the test specimens in all above-reported experiments, had large deflections and plastic deformations, finite element analyses had to be performed using the software offering combined geometrical and material non-linear capabilities. In this study, the commercially available finite element code, ANSYS [16] was adopted. In the control menu of ANSYS solver, the options of "large deflection" and "arc-length method" are activated. The arc-length method is used to trace the non-linear large deflection response of the models.

4.1. Shell element formulation

Both plate and stiffeners are modelled using SHELL43 elements selected from ANSYS library of elements. The SHELL43 element in Figure 9 is a so-called plastic large strain element and categorised in the family of four-node quadrilateral elements. Each node has three translational degrees of freedom in the nodal x, y and z directions as well as three rotational degrees of freedom about the nodal x, y and z-axes. The chosen element allows for elastic, perfectly plastic, with strain hardening or strain softening, large strain and large deflection response [16].
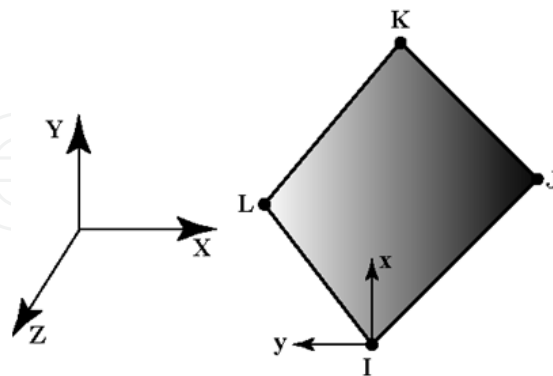
Figure 9. Shell43 element of the ANSYS FEM program

4.2. Finite element mesh and boundary conditions

A convergence study indicated that in the finite element mesh of isotropic and stiffened plates respectively, assuming $10 \times (a/b)$ mesh divisions along local plate panels and 10

mesh divisions across them is sufficient to capture accurately the buckling and plastic collapse behaviour. Respectively a and b represent the length and breadth of local plate panels. In order to model the stiffener's web and flange, respectively 6 to 7 and 5 to 6 elements are sufficient. However, the purpose of this study was to simulate the testing results and finer meshes were therefore used. In the case of Tanaka & Endo tests, to reduce the number of mesh divisions and speed up the time of analysis, a rational assumption was made. The transverse stiffeners or frames for the case of Tanaka & Endo tests were not modelled for simplicity; instead the nodes on the line of attachment of the transverse stiffeners were constrained from translational movement out of plate plane. Furthermore, the translational movements of these nodes along the axis perpendicular to the line of attachment of transverse stiffeners were coupled with each other. Transverse frames were modelled in the case of Ghavami's tests. In both Ghavami and Tanaka & Endo's tests, the stiffened plates were loaded in axial compression along the stiffeners. Also in their tests the simply supported boundary conditions were assumed in the models. Figs. 10 and 11 show typical finite element models with the simulated boundary conditions, used for the analysis of Tanaka & Endo test specimens and Ghavami P2L2T test specimen (as an example).
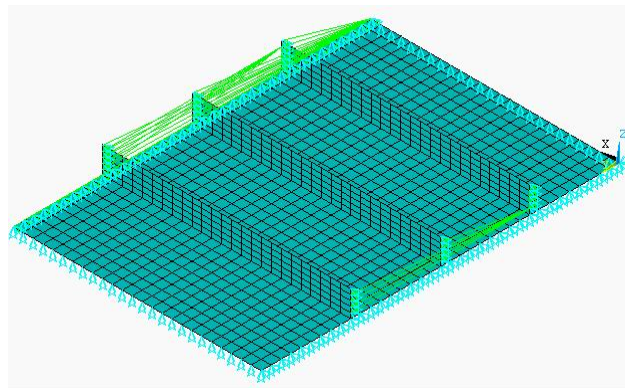

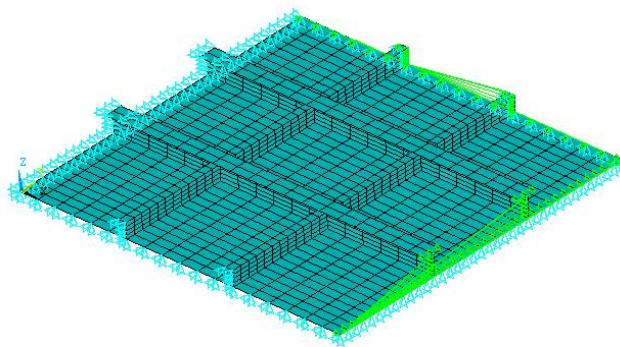**Figure 10.** Finite element model of Tanaka & Endo's test specimens

Figure 11. Finite element model of Ghavami's P2L2T test specimen

4.3 Imperfections

Welding residual stresses were not modelled specifically in this study. However, in order to simulate the complex pattern of residual welding stresses and initial deflections stated in

references [14] and [15], a special procedure was employed. Uniform lateral pressure was applied first on the stiffened plate model and a linear elastic finite element analysis was carried out. This analysis was repeated in a trial and error sequence of calculations so that the magnitude of maximum deflection of plate reached that, measured by Ghavami. It is assumed that this procedure would simulate both the residual welding stresses and initial geometrical imperfection. After satisfying this condition, the information concerning the coordinates of nodal points, element coordinates and boundary conditions was transferred to a new finite element mesh for the geometrical and material non-linear response analysis under the action of longitudinal in-plane compression.

It should be emphasised that the pattern of initial deflections induced in the Ghavami's specimens [14] were nearly matching the pattern produced by this procedure. For the case of Tanaka & Endo's tests, first an eigenvalue buckling analysis was made using ANSYS, in order to capture the three-wave buckling mode deflection of the specimens [15]. Then the deflection pattern in this mode was scaled to the same pattern with the maximum magnitude of initial deflection, A_{03}, (Table 4) before testing, which has been reported by Tanaka & Endo [15]. Nonlinear response analysis under the action of longitudinal in-plane compression was performed on this model.
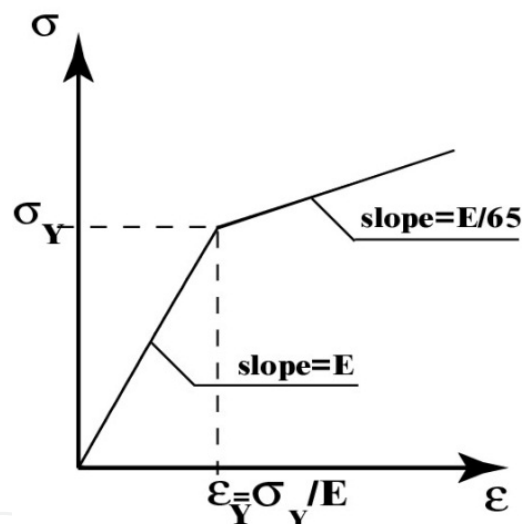

Figure 12. Assumed bi-linear behaviour for the material

4.4. Material properties

It is evident that strain-hardening effect has an important influence on the non-linear behaviour of isotropic and stiffened plates respectively. The degree of such an influence is a function of several factors including plate and stiffener slenderness. In this chapter, experimental material behaviour for both plate and stiffener are modelled as a bi- linear elastic-plastic with strain-hardening rate of $E/65$, as seen in Figure 12. E is modulus of elasticity of material. This value was obtained through an extensive study of elastic-plastic large deflection analyses made by Khedmati [17] and presents an average value for the strain-hardening rate. The application of $E/65$ predicts the collapse load with sufficient

accuracy. Poisson's ratio, ν, in all experimental investigation and FEM analysis was considered to be equal to 0.3.

5. Large deflection behaviour of the tested plates

A summary of the results obtained through the finite element simulation of the experimental research carried out by Ghavami is given in Tables 5 and 6 and that of Tanaka & Endo is presented in Table 7. In these tables, the collapse modes from FEM analyses are, also, presented. A comparison of the experimental and those obtained results from FEM results present a very good agreement. The maximum differences varied between 16 percents and 22 percents for the series II and III (Table 5) of Ghavami's experimental result. These two extreme differences are related to the plates with L shape stiffener, which does not have a symmetrical geometrical shape. The simple assumption considered in the FEM simulation of complex pattern of initial imperfections (including both initial deflections and welding residual stresses) inherent in the experimental investigation, in addition to not having perfect simply supported boundary conditions in these two series must have led to those higher discrepancies. It should be emphasized that it was possible to trace the curve of average stress-average strain relationship for any combination of plate and stiffener. Finite element simulation results for Ghavami's test models without transverse frame show that the collapse has occurred following the buckling instability of local plate panels (Table 5). This was well predicted by FEM for test specimen P2R with only 5 percent difference. Detailed information concerning the behaviour of each of the Ghavami's test specimens are well documented in the References [18-22].

In the analysis of Tanaka & Endo's tests, the longitudinally stiffened plate located in the middle of the test specimens were simulated assuming all edges straight and having simply supported conditions. The same boundary conditions were considered in FEM analysis. In such cases, finite element simulation results, described also well the interactive buckling of plates and stiffeners in most of the cases, (Table 7). The smallest value of stiffener web height-to-web thickness ratio belongs to model D3, while the biggest value of this ratio corresponds to models D4 and D4A. Model D3 has failed due to local deformation in the plate, while in the case of models D4 and D4A the collapse has been produced by large plastic deformations both in the plate and stiffeners. Interactive buckling in both plate and stiffeners can be observed in other models, where the level of plastic deformations, in the plate varies among them. The ultimate strength predicted by FEM are well consistent as compared with those obtained by Tanaka & Endo [15]. This could be related to the initial deflection of the test specimens which was presented in FEM with a good accuracy.

A summary of results for three tests from each series of VI, V and VI that had perfect simply supported boundary is presented in Table 6. It can be noted that the difference between FEM and those of experimental results had only a difference of up to 5 percent. In the following, the results of FEM for P1R1T, P2R1T and P2L2T of the Ghavami's models with transverse frame are discussed in details.
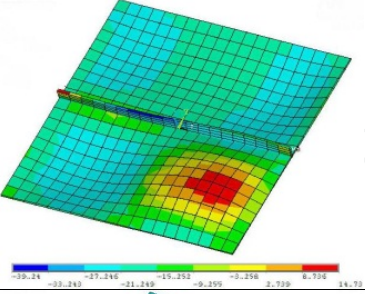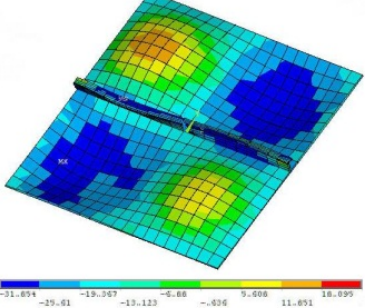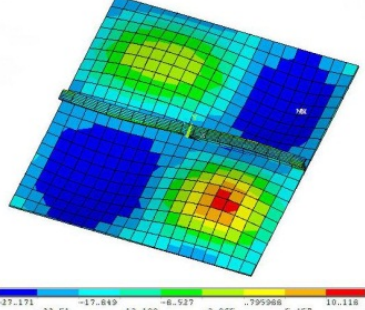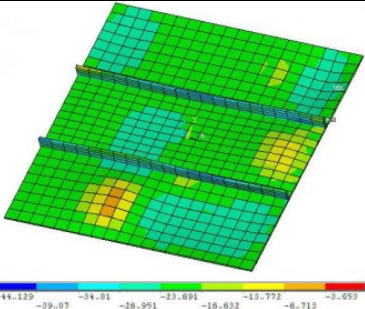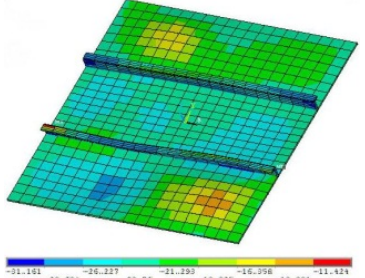
Test model	$\dfrac{(\sigma_{ult})_{FEM}}{(\sigma_{ult})_{EXPERIMENT}}$	Collapse mode
P1R	1.11	
P1L	0.84	
P1T	0.87	
P2R	1.05	
P2L	1.22	

Table 5. Summary of finite element simulation results for some of Ghavami test models without transverse frame

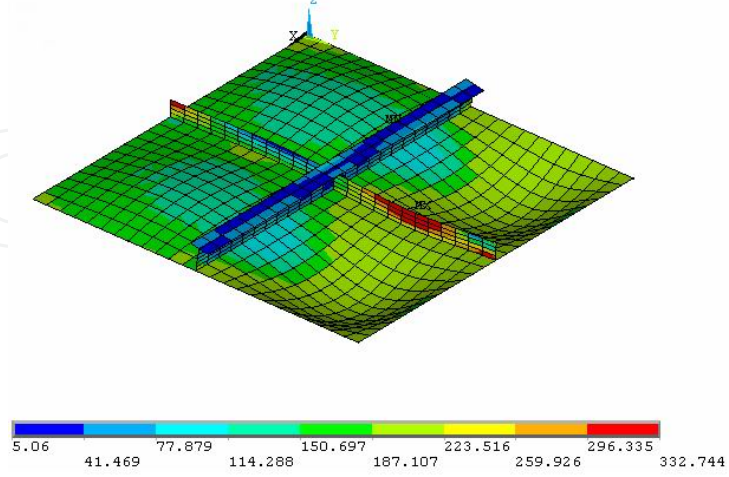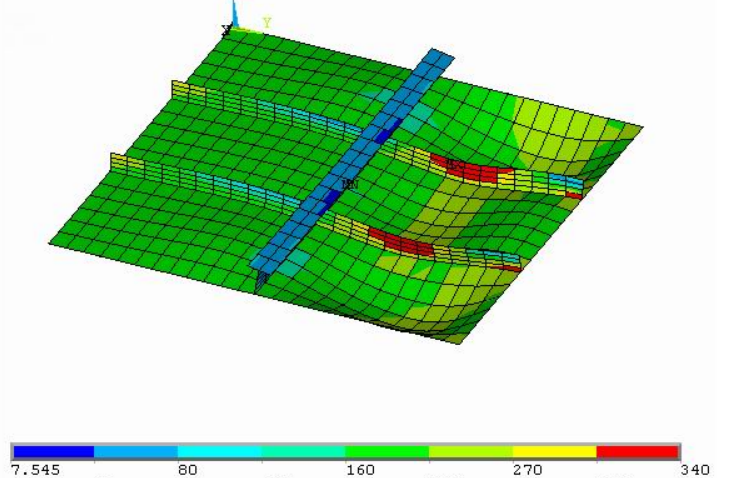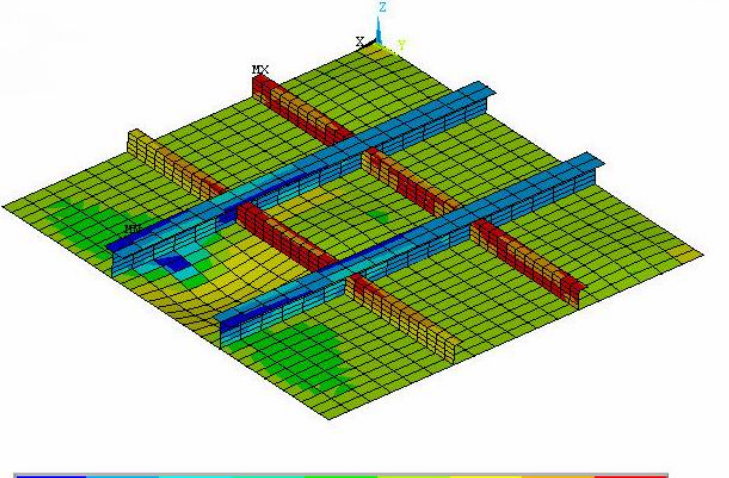| Test model	$\dfrac{(\sigma_{ult})_{FEM}}{(\sigma_{ult})_{EXPERIMENT}}$	Collapse mode
P1R1T	1.05	
P2R1T	1.02	
P2L2T	1.02	

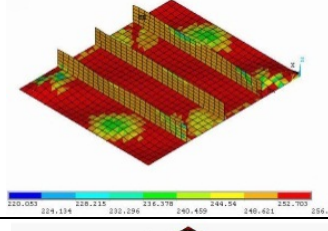**Table 6.** Summary of finite element simulation results for some of Ghavami test models with transverse frame
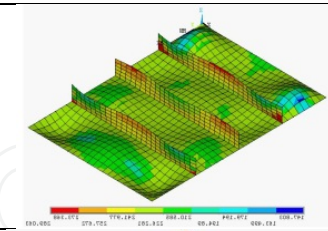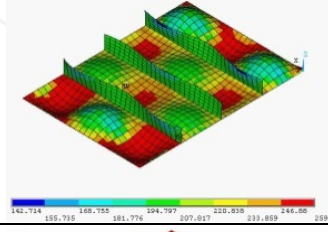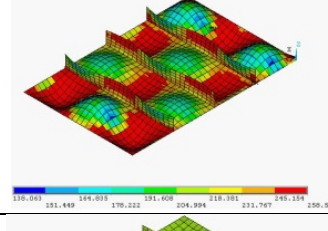
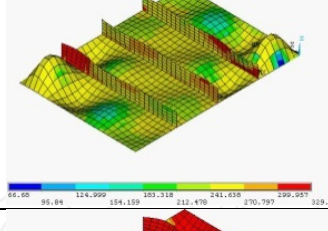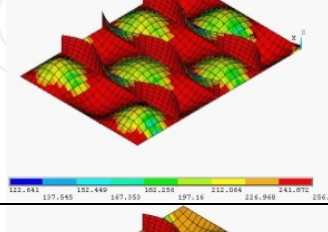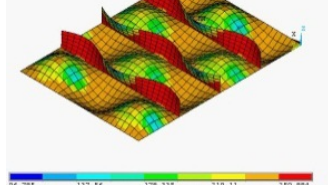| Structure No.	Tanaka & Endo	Present	
	$\dfrac{(\sigma_{ult})_{FEM}}{(\sigma_{ult})_{EXPERIMENT}}$	$\dfrac{(\sigma_{ult})_{FEM}}{(\sigma_{ult})_{EXPERIMENT}}$	Collapse mode
D0	0.977	1.014	
D0A	1.028	1.065	
D1	0.869	0.911	
D2	0.936	0.944	
D3	0.860	0.853	
D4	0.792	0.866	
D4A	0.866	0.960	

Table 7. Summary of results for some of Tanaka & Endo tests

5.1. P1R1T Ghavami model

The relative undimensional average stress-average strain relationship obtained by FEM analysis for P1R1T model is shown in Figure 13. The P1R1T model failed because of torsional buckling and plastic failure mechanism of the longitudinal stiffener (R). The torsional failure of the stiffener is induced in the FEM model shortly before the collapse of the model due to work softening as can be seen in Figure 13. A comparison between the collapse modes of the experimental model, Figure 14 (left) and that of FEM analysis, Figure 14 (right) is presented. It can be observed that the simulation of plate deformations by FEM analysis is almost identical to the failure mode occurred in the test specimen. The work hardening of the model started at about $\varepsilon/\varepsilon_y$ =0.8 and reached the ultimate buckling stress at $\varepsilon/\varepsilon_y$ =1.0 (ε, ε_y is the average strain and the yield strain respectively). The ultimate buckling strength of this model is about 80 percent of the plate yield strength, as can be seen in Figure 13 in turn it is close to the experimental results presented in Table 3. The FEM result overestimated the experimental one by only 5 percent. This mainly could be related to the discrepancy in the consideration of initial welding and initial deflection in REM analysis.
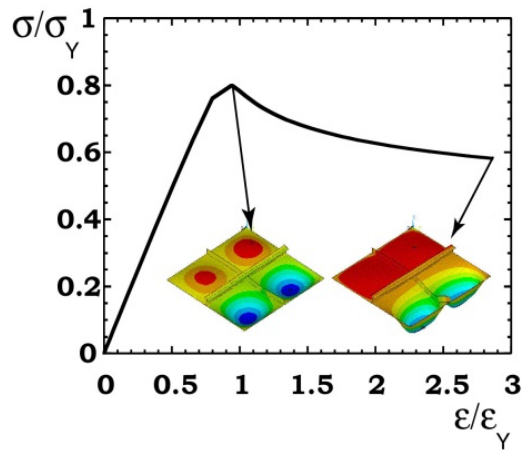

Figure 13. Average stress-average strain relationship and spread of yielding at collapse and final step of calculation for Ghavami P1R1T model
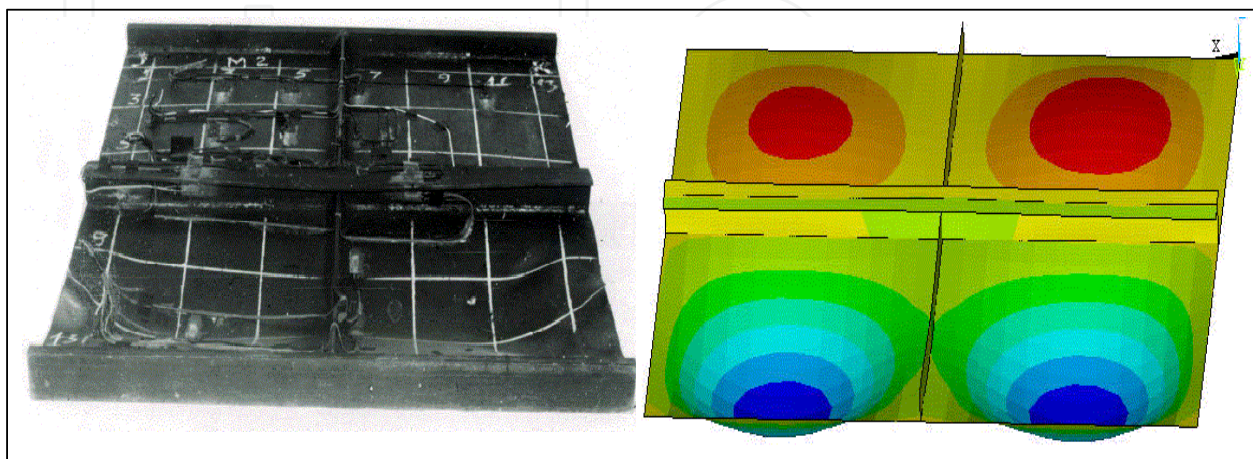

Figure 14. Deflected mode at collapse for Ghavami P1R1T model obtained by experiment (left) and FEA (right)

5.2. P2R1T Ghavami model

As it can be seen from the relative average stress-average strain relationship of P2R1T model (Figure 15), the work hardening of the test model started at about $\varepsilon/\varepsilon_y$ =0.8 and reached the ultimate buckling stress at $\varepsilon/\varepsilon_y$ =0,93 percent in relation to the plate material yield strength. Then the work softening or unloading started at $\varepsilon/\varepsilon_y$ =1.0 together with the local plastic deformations in the post-ultimate buckling region. The P2R1T model failed under axial compression load due to the buckling in both plate and stiffeners. Such a failure was predominant in upper part of the transverse T frame, as can be observed in Figure 16 (left). In the lower part of the transverse T stiffener, the plastic deformation in the plate and stiffeners was not very large. The comparison of FEM results with that of the experimental one, presented in Figure 16 present a relatively perfect prediction of the ultimate buckling modes. The FEM result overestimated the experimental one by only 2 percent. This can be also related mainly to consideration of the initial welding and initial deflection in the FEM analysis.
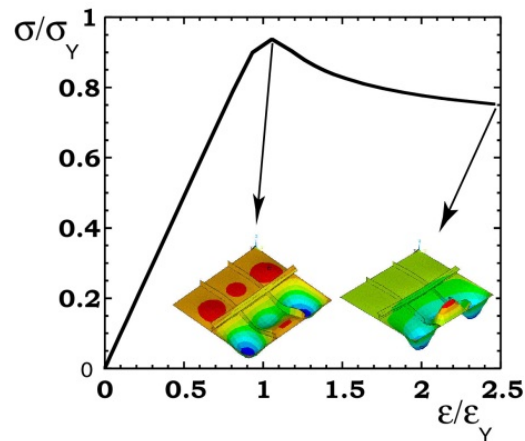

Figure 15. Average stress-average strain relationship and spread of yielding at collapse and final step of calculation for Ghavami P2R1T model
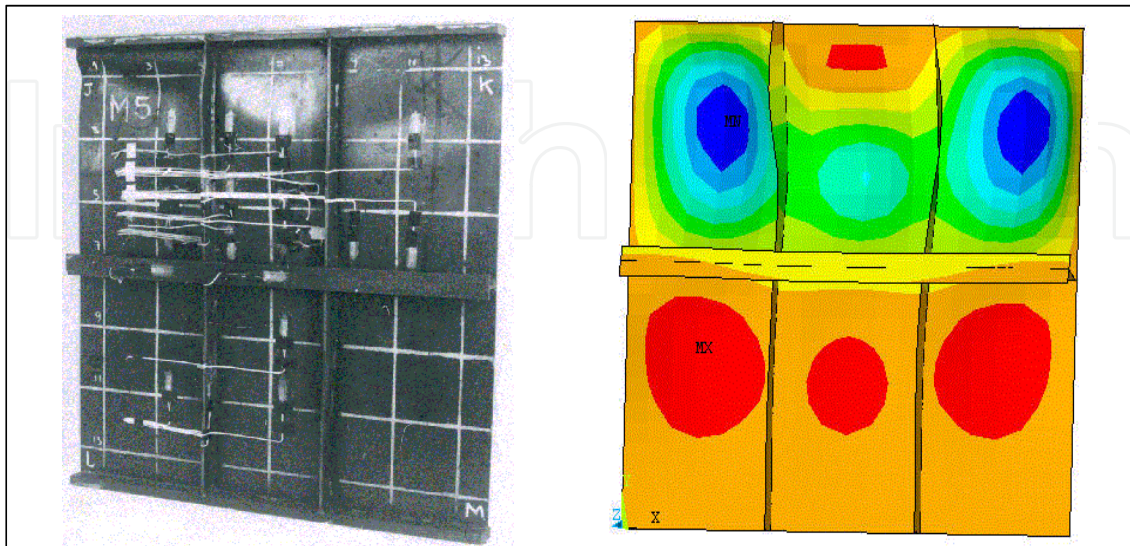

Figure 16. Deflected mode at collapse for Ghavami P2R1T model obtained by experiment (left) and FEA (right)

5.3. P2L2T Ghavami model

As it can be seen in Figure 17 which presents the relative average stress-average strain, relationship of P2R2T model, a small work hardening started at about $\varepsilon/\varepsilon_y$ =0.88 of the plate yield stress and reached the ultimate buckling stress of 100 percent. Then a plastic deformation started at the $\varepsilon/\varepsilon_y$ =1.0 up to $\varepsilon/\varepsilon_y$ =1.7 generating several local plate. After this stage the work softening or unloading started with the expansion of local plastic deformations in the post-ultimate buckling region. The P2R2T model finally failed due to the buckling induced in both plate and longitudinal L stiffeners in the centre of the stiffened plate as can be noted well in Figure 18 (left). The P2L2T model showed a high strength under in-plane compression load. The FEM deflected form in Figure 18 (right) simulated well the experimental results. The FEM result overestimated the experimental one by only 2 percent as can be seen in Table 6. This could be related principally to the initial welding and initial deflection.
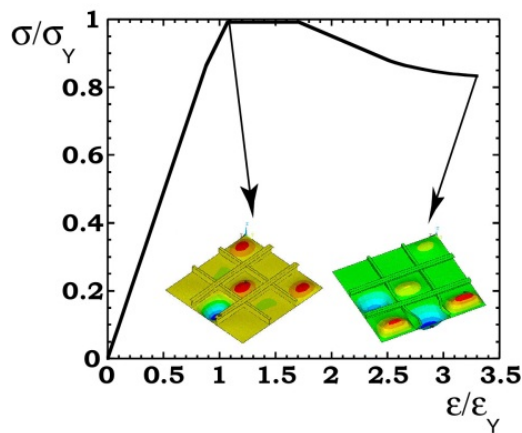

Figure 17. Average stress-average strain relationship and spread of yielding at collapse and final step of calculation for Ghavami P2L2T model
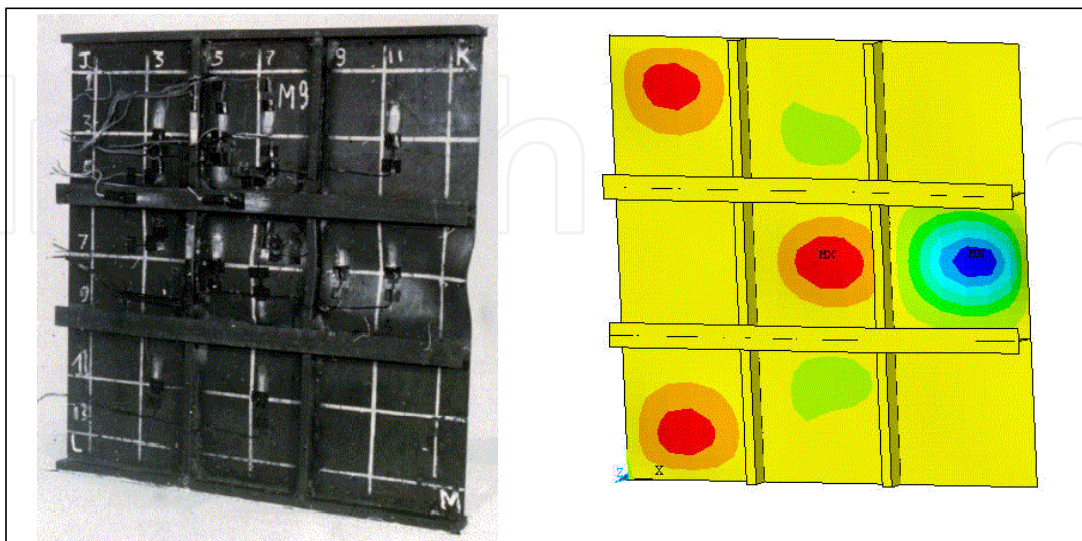

Figure 18. Deflected mode at collapse for Ghavami P2L2T model obtained by experiment (left) and FEA (right)

6. Large deflection behaviour of Stiffened plates subjected to combined in-plane compression and lateral pressure

For the stiffened plates in the bottom structure of ships, the basic load case for buckling design consists of the following loads applied simultaneously (Figure 19):

• longitudinal compression arising from the overall hull girder bending,
• transverse compression arising from the bending of double bottom under lateral pressure, and
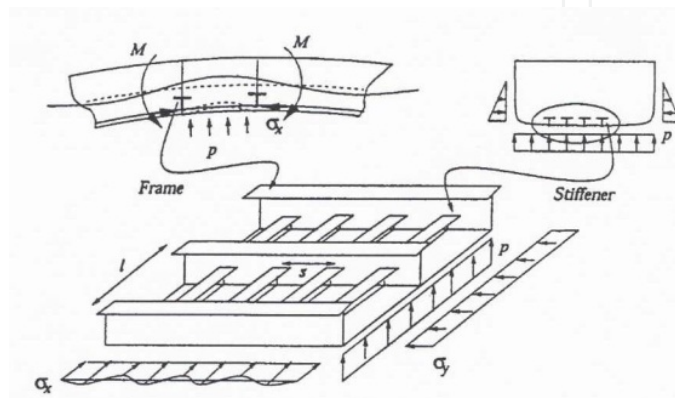• local bending arising from the direct action of lateral pressure.

Figure 19. Basic loads applied on ship stiffened plates

The continuous plate was assumed to be simply-supported along the stiffener lines with no out-of-plane deflection. In reality, however, the stiffener is also subjected to lateral pressure, and it may collapse prior to the failure of the panels. The focus of the present chapter is concentrated on the buckling and plastic collapse behaviour of continuously stiffened plates subjected to combined biaxial compression and lateral pressure with the main objective of identification of the collapse modes of the plates subjected to mentioned combination of loading condition.

A series of elasto-plastic large deflection FEM analyses is performed on continuous stiffened plates with flat-bar, tee-bar, and angle-bar stiffeners of the same flexural rigidity. The buckling/plastic collapse behaviour and ultimate strength of stiffened plates are hereby assessed so that both the material and geometrical nonlinearities are taken into account.

Local plate panels with length, a, of 2400 mm and breadth, b, of 800 mm are considered, and their thickness, t, changes from 13mm, 15mm, and 20 mm. Yield stress of the material, σ_Y, is taken as 313.6 MPa, and bilinear stress-strain relationship is assumed with the kinematical strain-hardening rate of $E/65$, where E is Young's modulus of the material. E is considered as 205.8GPa. The cross-sectional geometries of stiffeners are given in Table 8. In each group, the stiffeners have the same moment of inertia. A triple span-double bay model is applied for the analysis of buckling/plastic collapse behaviour of continuous stiffened plate with symmetrical stiffeners (ABDC in Figure 20). When a stiffener has an unsymmetrical geometry, a triple span-triple bay model is used (ABFE in Figure 20) [23].

Type	Model	shape	h_w	t_w	b_f	t_f	h_w/t_w
1	F1	flat	150	17	-	-	8.82
1	T1	tee	150	9	90	12	16.67
1	A1	angle	150	9	90	12	16.67
2	F2	flat	250	19	-	-	13.16
2	T2	tee	250	10	90	15	25.00
2	A2	angle	250	10	90	15	25.00
3	F3	flat	350	35	-	-	10.00
3	T3	tee	400	12	100	17	33.33
3	A3	angle	400	12	100	17	33.33

h_w: Height of stiffener web (mm)
t_w: Thickness of stiffener web (mm)
b_f: Breadth of stiffener flange (mm)
t_f: Thickness of stiffener flange (mm)

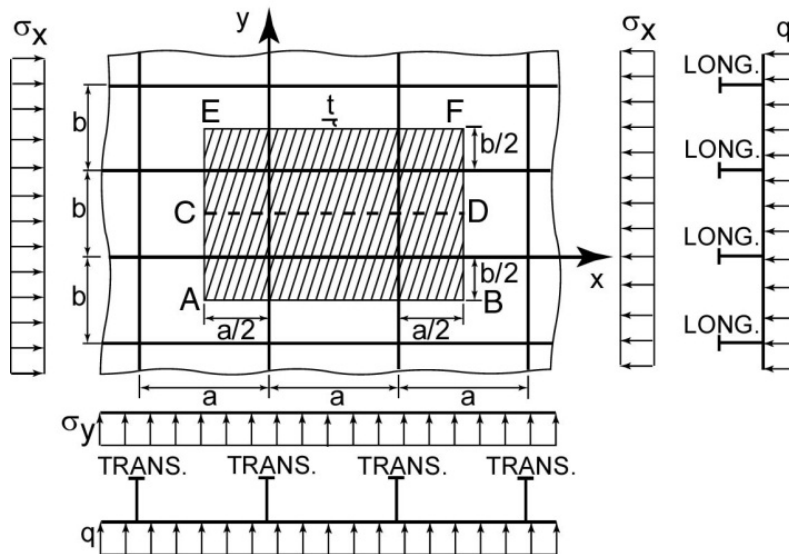**Table 8.** Cross-sectional geometries of stiffeners

Figure 20. Stiffened plate model for FEM analysis

The considered boundary conditions are as follows:

- Periodically continuous conditions are imposed at the same y-coordinate along the transverse edges (i.e. along AC and BD in double bay model and along AE and BF in triple bay model).
- Symmetry conditions are imposed along the longitudinal edges of double bay model (i.e. along AB and CD). But periodically continuous conditions are defined at the same x-coordinate along the longitudinal edges of triple bay model (i.e. along AB and EF).
- Although transverse frames are not modelled, the out-of-plane deformations of plate and stiffener are restrained along the junction lines of them and the transverse frame.
- To consider the plate continuity, in-plane movement of the plate edges in their perpendicular directions is assumed to be uniform.

The lateral pressure ranging from 0 to 60 metres water head initially is applied up to a specified value always perpendicularly to the plate surface. Then biaxial compression is exerted proportionally by uniform forced displacements.

Three types of initial imperfections as described in the following are accounted for:

- initial deflection in the plate with the maximum magnitude of t /100 (Figure 21(a)):

$$W_{p0} = \frac{t}{100} \sin \frac{m\pi x}{a} \sin \frac{\pi y}{b}$$ (3)

where m is the number of buckling half-waves in the plate,

- initial deflection in the stiffener with the maximum magnitude of a /1000 (Figure 21(b)):

$$W_{s0} = \frac{a}{1000} \sin \frac{\pi x}{a}$$ (4)

- and angular distortion of the stiffener which is taken as (Figure 21(c)):

$$\phi_0 h_w = \frac{a}{1000} \sin \frac{\pi x}{a}$$ (5)

The welding residual stresses are not considered.

(a) Initial deflection in the plate   (b) Initial deflection in the stiffener   (c) Angular distortion of the stiffener
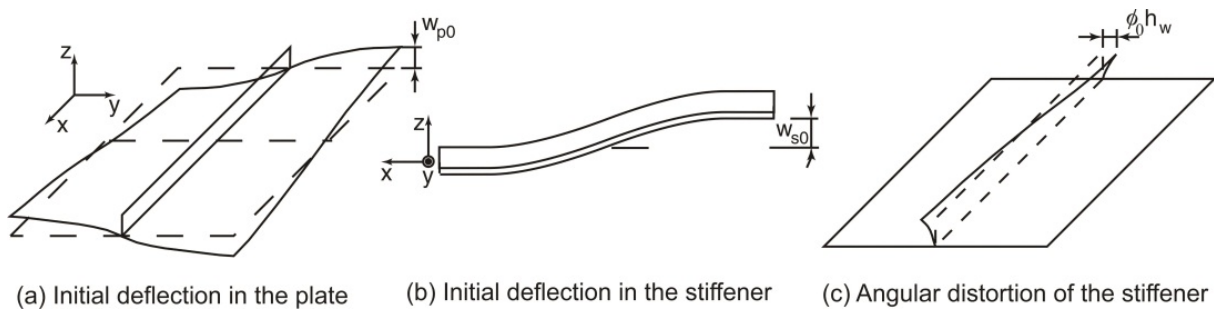
Figure 21. Initial imperfections in the stiffened plate models

6.1. Plates with flat-bar stiffener subjected to combined longitudinal compression and lateral pressure

Average stress-average strain relationships for continuous stiffened plates with flat-bar stiffeners subjected to combined longitudinal compression and variable levels of lateral pressure, are shown in Figure 22 for the plate thickness of t =13 mm. The deflection mode and spread of yielding at ultimate strength are presented in Figure 23.

The characteristics of the collapse behaviour can be summarised as follows:

- When there is no lateral pressure (water head, h =0 m), the stiffened plate under longitudinal compression collapses in Eulerian buckling mode, preceded by the local buckling of plate with three buckling half waves.

- With increase in lateral pressure, the deflection mode at the ultimate strength changes from the Eulerian buckling mode to a both-ends clamped mode, and the tripping deformation of stiffener gets decreased.
- Under very high lateral pressure, the stiffener web is fully yielded at both ends of each span, and subsequently it is deflected entirely to opposite sideward directions in neighbouring spans. Therefore, a kind of simply-supported flexural-torsional deformation is produced in the stiffener web.
- With an increase in the flexural rigidity of the stiffener, ultimate strength of the stiffened plate is increased with a decrease in the post-ultimate strength.
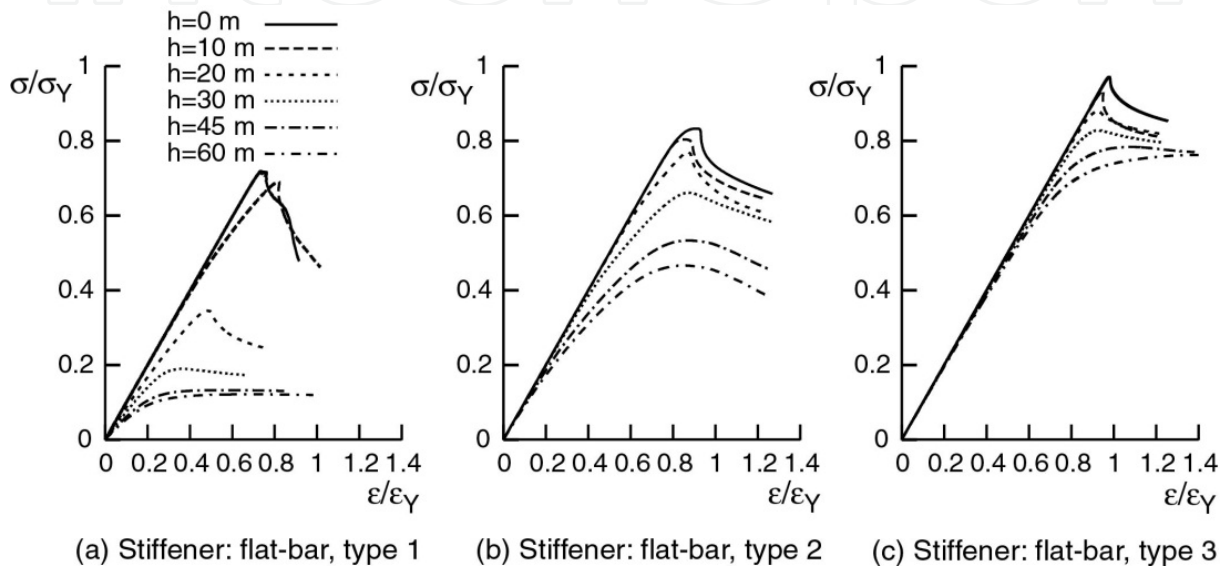

(a) Stiffener: flat-bar, type 1   (b) Stiffener: flat-bar, type 2   (c) Stiffener: flat-bar, type 3

Figure 22. Comparison of average stress-average strain relationships for a continuous stiffened plate under combined longitudinal thrust and lateral pressure (plate: 2400x800x13 mm)
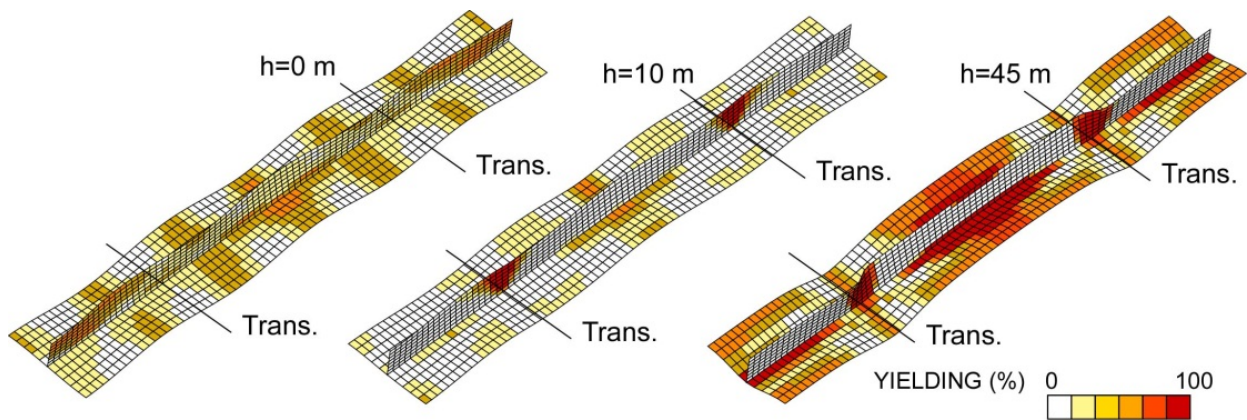

Figure 23. Change in the deflection mode at ultimate strength for a continuous stiffened plate under combined longitudinal thrust and lateral pressure (plate: 2400x800x13 mm, stiffener: flat-bar of type 2)

For plates with flat-bar stiffeners of type 1 having smaller flexural rigidity, as the plate thickness is increased, the ultimate strength is increased with the increase of lateral pressure up to a certain value. This is because the collapse mode changes from Eulerian buckling mode to a clamped mode in which the plate itself exhibits a higher resistance to longitudinal

compression. With a further increase in the applied lateral pressure, however, the deteriorating effect of lateral pressure, i.e. enhancing yielding at stiffener becomes more predominant and the ultimate strength starts to decrease considerably.

6.2. Plates with tee-bar stiffener subjected to combined longitudinal compression and lateral pressure

Average stress-average strain relationships for continuous stiffened plates with tee-bar stiffeners of type 2 subjected to combined longitudinal compression and variable levels of lateral pressure, are shown in Figure 24(a) for the plate thickness of t =13 mm. Fundamental collapse behaviours and ultimate strength of stiffened plates with tee-bar stiffeners are almost the same as those for the flat-bar stiffener, but strength reduction in the post-ultimate range is smaller comparing with Figure 22(b). This is because the horizontal bending rigidity of tee-bar is much greater than that of flat-bar.
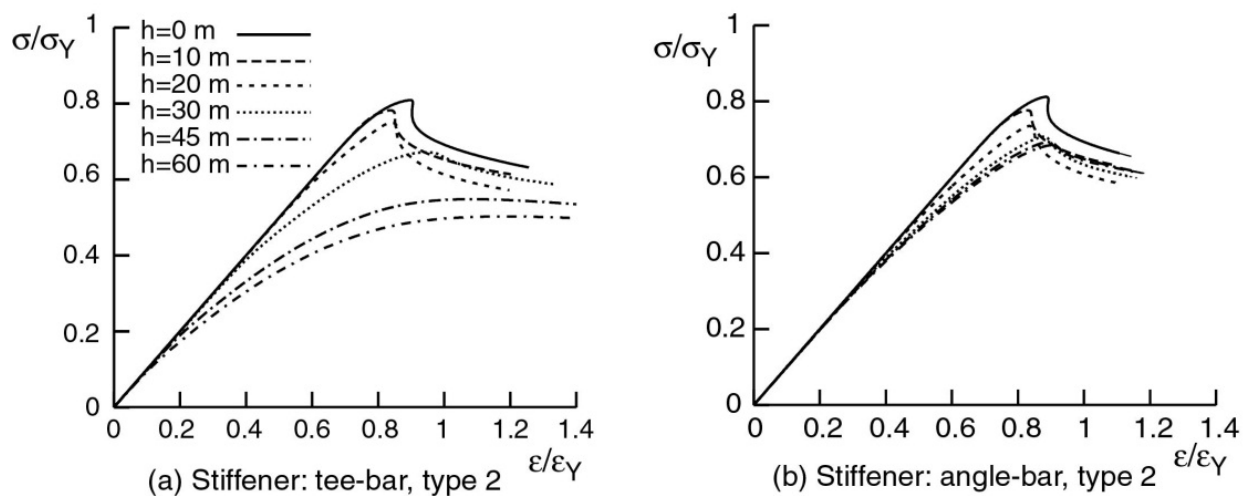

Figure 24. Comparison of average stress-average strain relationships for a continuous stiffened plate under combined longitudinal thrust and lateral pressure (plate: 2400x800x13 mm)

6.3. Plates with angle-bar stiffeners subjected to combined longitudinal compression and lateral pressure

Average stress-average strain relationships and collapse modes obtained for the continuous stiffened plates with angle-bar stiffeners are shown in Figure 24(b) and Figure 25, respectively, for the plate thickness of t =13 mm.

Unlike the flat-bar or tee-bar stiffeners having symmetrical cross-sectional shape, the angle-bar stiffener deflects to the same horizontal and vertical directions in all adjacent spans (Figure 25). This flexural-torsional deflection of stiffener clamped at both ends constrains the panel deformation, resulting in larger ultimate strength and smaller strength reduction in the post-ultimate range than those for flat-bar or tee-bar stiffeners.
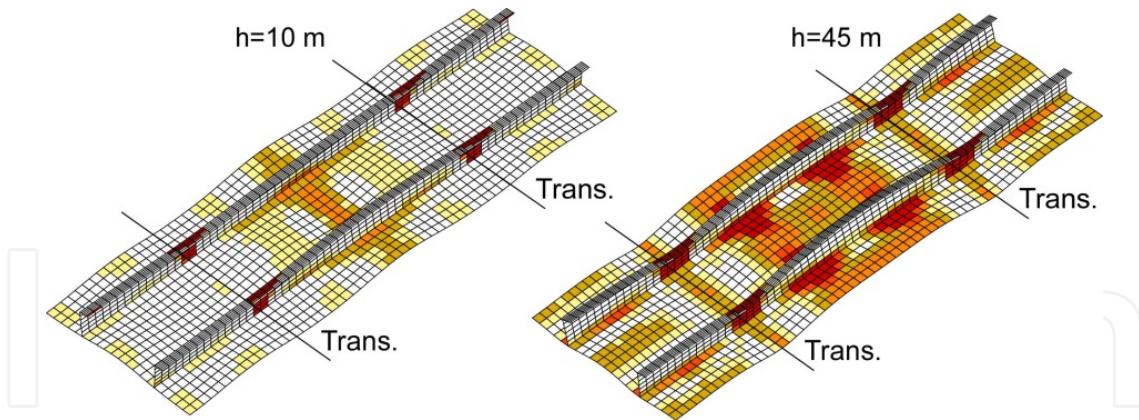
Figure 25. Change in the deflection mode at ultimate strength for a continuous stiffened plate under combined longitudinal thrust and lateral pressure (plate: 2400x800x13 mm, stiffener: angle-bar of type 2)

It is to be noted here that although an angle-bar stiffener is quite effective from the viewpoint of buckling/plastic collapse strength, it should be carefully used from the view point of fatigue strength [24].

6.4. Stiffened plates subjected to combined transverse compression and lateral pressure

The results for the continuous stiffened plates with flat-bar stiffeners of type 2 subjected to combined transverse compression are shown in Figs. 26 and 27.
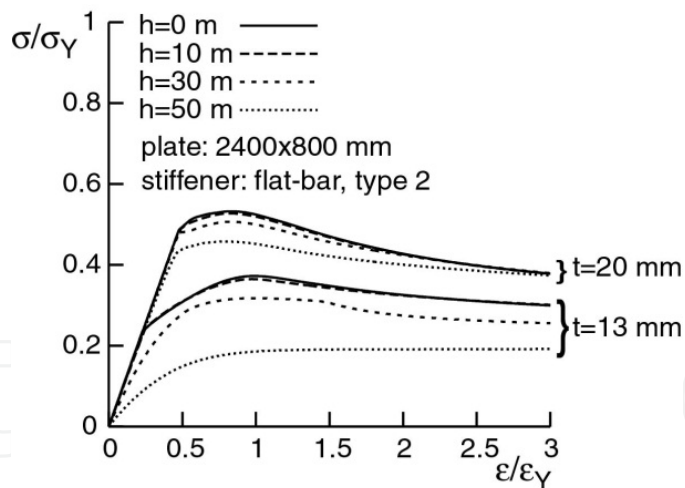

Figure 26. Comparison of average stress-average strain relationships for a continuous stiffened plate under combined transverse thrust and lateral pressure

When lateral pressure is small, the local rectangular panels collapse as if they were simply-supported along the edges, accompanied by some rotation of stiffeners. With an increase in lateral pressure, the collapse mode changes from the simply-supported mode to the all-edges clamped mode. These behaviours are basically the same as those observed for continuous plate simply-supported along stiffener lines. Since the stiffener is not subjected to compression, its deflection is small compared to the panel deflection.
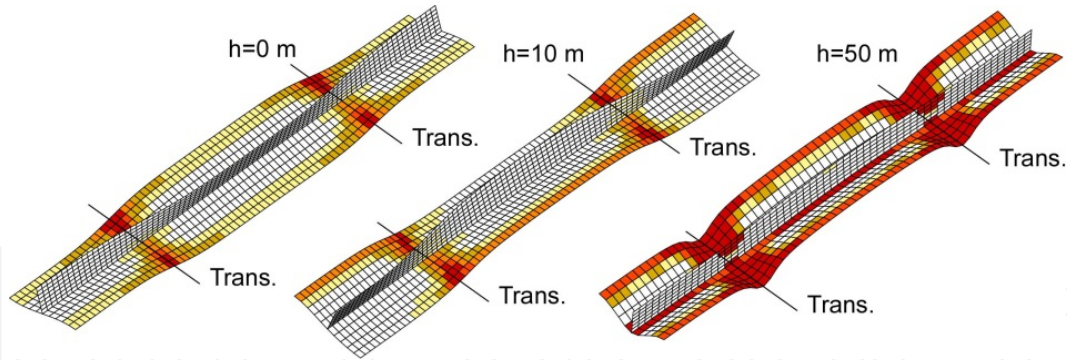
Figure 27. Change in the deflection mode at ultimate strength for a continuous stiffened plate under combined transverse thrust and lateral pressure (plate: 2400x800x13 mm, stiffener: flat-bar of type 2)

6.5. Stiffened plates subjected to combined biaxial compression and lateral pressure

A series of FEM analyses is performed on a continuous stiffened plate with flat-bar stiffeners subjected to combined biaxial compression and lateral pressure. The results are shown in Figure 28. The dotted lines are loading paths for different ratios of applied biaxial displacements. The solid line is the obtained envelope of all loading paths representing the ultimate strength interaction curve.
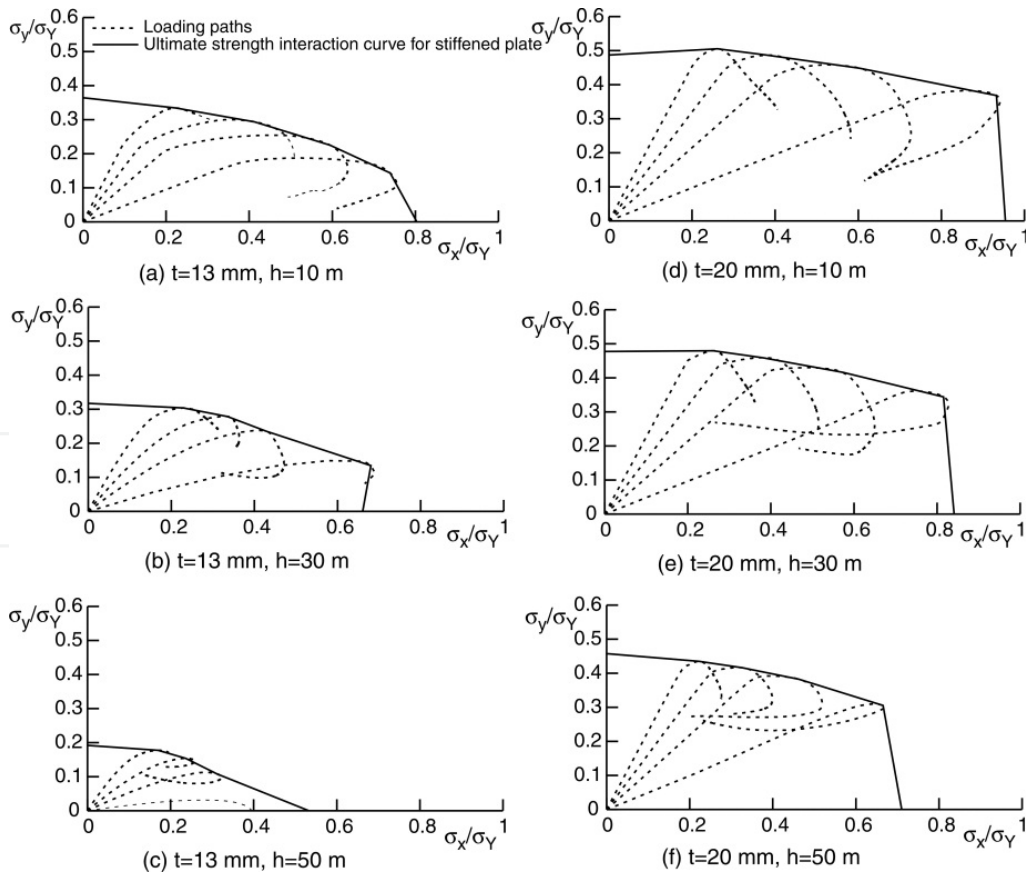

Figure 28. Interaction curves for a continuous stiffened plate subjected to combined biaxial thrust and lateral pressure (plate: 2400x800 mm, stiffener: flat-bar of type 2)

It is seen that each interaction curve basically consists of two parts; a semi-horizontal region in which the stiffened plate behaves as if it were under combined transverse compression and lateral pressure, and a semi-vertical region where the behaviour as in the case of combined longitudinal compression and lateral pressure is dominant.

7. Conclusion

Basing the results of this chapter on the analysis of 29 experimental investigation, on stiffened steel plates subjected to uniform axial compression load up to final failure, by the Finite Element program ANSYS, the following conclusions may be drawn. The selected element SHELL43, could trace full-range, elastic-plastic behaviour of the stiffened plates. The capability of the non-linear FEM to perform the analysis of stiffened plates has been demonstrated through the accurate simulation of the Ghavami and Tanaka & Endo tests. Although some simplifying assumptions for the simulation of initial imperfections and residual welding stresses were made for reducing the calculation volume and speeding up the analysis, the accuracy of the collapse load obtained through FEM simulations is relatively in good consistency with the test results. The differences were higher in cases of not having perfect simply supported boundary conditions as in series II and III of Ghavami's test. It was shown also, that obtaining deflection mode is possible at any step of loading. This allows predicting the local buckling of stiffened plates with relatively good precision.

For small value of lateral pressure, the local panel and stiffener tend to collapse in a simply-supported mode. With an increase in the applied pressure, they are likely to fail in a clamped mode. Angle-bar stiffener has larger stiffening effects than those of flat-bar and tee-bar stiffeners having the same flexural rigidity, from the view point of ultimate strength.

Author details

Khosrow Ghavami
Department of Civil Engineering, Pontificia Universidade Católica (PUC-Rio), Rio de Janeiro, Brazil

Mohammad Reza Khedmati[*]
Faculty of Marine Technology, Amirkabir University of Technology, Tehran, Iran

Acknowledgement

8. References

[1] Merrison Committee (1973) Inquiry into Basis of Design and Methods of Erection of Steel Box Girder Bridges. Report of the Committee – Appendix 1: Interim Design and Workmanship Rules. Her Majesty's Stationary Office, London.

[*] Corresponding Author

[2] Crisfield MA (1975) Full-range Analysis of Steel Plates Stiffened Plating under Uniaxial Compression. Proc. Civ. Engrs. 59(2): 595-624.

[3] Frieze PA, Dowling PJ, Hobbs RE (1976) Ultimate Load Behaviour of Plates in Compression. Proc. International Conference on Steel Plated Structures, Imperial College, London.

[4] Brosowski B, Ghavami K. (1996) Multi-Criteria Optimal Design of Stiffened Plates. Part I, Choice of the Formula for Multi-Criteria for Buckling Load. Thin Walled Structures. 24(9): 353-369.

[5] Brosowski B, Ghavami K. (1997) Multi-Criteria Optimal Design of Stiffened Plates. Part II, Mathematical Modelling of the Optimal Design of Longitudinally Stiffened Plates. Thin Walled Structures. 28(2): 179-198.

[6] Murray NW. (1975) Analysis and Design of Stiffened Plates Collapse Load. The Structural Engineer. 53(3): 153-158.

[7] Chen Q, Zimmerman TJE, DeGeer D, Kennedy BW. (1997) Strength And Stability Testing of Stiffened Plate Components. Ship Structural Committee Report. SSC-399.

[8] Hu SZ, Jiang L. (1998) A Finite Element Simulation of the Test Procedure of Stiffened Plates. Journal of Marine Structures. 11: 75-99.

[9] ADINA-IN for ADINA Users Manual. (1990) Report ARD 90-4, ADINA R&D, Inc.

[10] Vibration and Strength Analysis Program (VAST) User's Manual, Version 7.2. (1996) Martec Limited, Halifax, Nova Scotia, Canada, 1996.

[11] Grondin GY, Elwi AE, Cheng JJR. (1999) Buckling of stiffened plates- a parametric study. Journal of Constructional Steel Research. 50: 151-175.

[12] Hibbitt et al. ABAQUS/Standard, Version 5.4. (1994) Hibbitt, Karlsson and Sorensen, Inc.: Pawtucket, RI.

[13] Sheikh IA, Elwi AE, Grondin GY. (2003) Stiffened Steel Plates under Combined Compression and Bending. Journal of Constructional Steel Research. 59: 911-930.

[14] Ghavami K. (1994) Experimental Study of Stiffened Plates in Compression up to Collapse. Journal of Constructional Steel Research. 28(2): 197-222 [Special Brazilian Issue, Guest Editor Khosrow Ghavami]

[15] Tanaka Y, Endo H. (1988) Ultimate Strength of Stiffened Plates with Their Stiffeners Locally Buckled in Compression. Journal of the Society of Naval Architects of Japan. 164 (in Japanese).

[16] ANSYS User's Manual (version 7.1). (2003) Swanson Analysis Systems Inc. Houston,.

[17] Khedmati MR. (2000) Ultimate Strength of Ship Structural Members and Systems Considering Local Pressure Loads. Dr. Eng. Thesis, Graduate School of Engineering, Hiroshima University.

[18] Ghavami K, Conci A, Rocha SAS. (1983) Resistencia Compressao De Placas De Aco Enrijecidas Longitudinalmente. In Proc. VII Congress Brasileiro de Engenharia Mecanica-COBEM 83, Uberlandia, Brasil: 339-349.

[19] Ghavami K, Conci A, Rocha SAS. (1983) Metodos De Calculo De Placas Enrijecidas Sob Carregamento De Compressao Axial. In Proc. VII Congress Brasileiro de Engenharia Mecanica-COBEM 83, Uberlandia, Brasil: 351-361.

[20] Conci A. (1983) Instabilidade Ate O Colapso De Placas De Aco Enrijecidas Em Dual Direcoes. MSc thesis, Pontificia Universidade Catolica, Rio de Janeiro.

[21] Rocha SAS. (1982) Comportamento Ultimo De Placas Enrijecidas. MSc thesis, Pontificia Universidade Catolica, Rio de Janeiro.

[22] Ghavami K. (1986) The Collapse of Continuously Welded Stiffened Plates Subjected to Uniaxil Compression Load. In Proc. Inelastic Behaviour of Plates and Shells, Simp. Rio de Janeiro, 1985, eds. L. Bevilacqua, R. Feijoo & R. Valid, Springer Berlin: 404-415.

[23] Yao T, Fujikubo M, Yanagihara D, Irisawa M. (1998) Consideration on FEM Modelling for Buckling/Plastic Collapse Analysis of Stiffened Plates. Trans. of the West-Japan Soc. Naval Arch. 85:121-128 (in Japanese).

[24] Kawano H, Kuramoto Y, Sakai D, Hashimoto K, Inoue S, Fushimi A, Hagiwara K. (1992) Some Considerations on Basic Behaviour of Asymmetric Sectional Frame Under Uniform Pressure. Trans. of the West-Japan Soc. Naval Arch. 83:161-166 (in Japanese).